Electronic Supplementary Information

for

Biobased thin-film composite membranes comprising priamine–genipin selective layer on nanofibrous biodegradable polylactic acid support for oil and solvent-resistant nanofiltration

Cong Yang[1], Fuat Topuz[1], Sang-Hee Park[1,2], Gyorgy Szekely[1*]

[1]Advanced Membranes and Porous Materials Center, Physical Science and Engineering Division (PSE), King Abdullah University of Science and Technology (KAUST), Thuwal, 23955-6900, Saudi Arabia

[2]Department of Chemical Engineering, Changwon National University (CNU), Changwon 51140, Korea

[*]Corresponding author: E-mail: gyorgy.szekely@kaust.edu.sa; Web: www.szekelygroup.com

Table of Contents

S1. Green nanofibrous support optimization

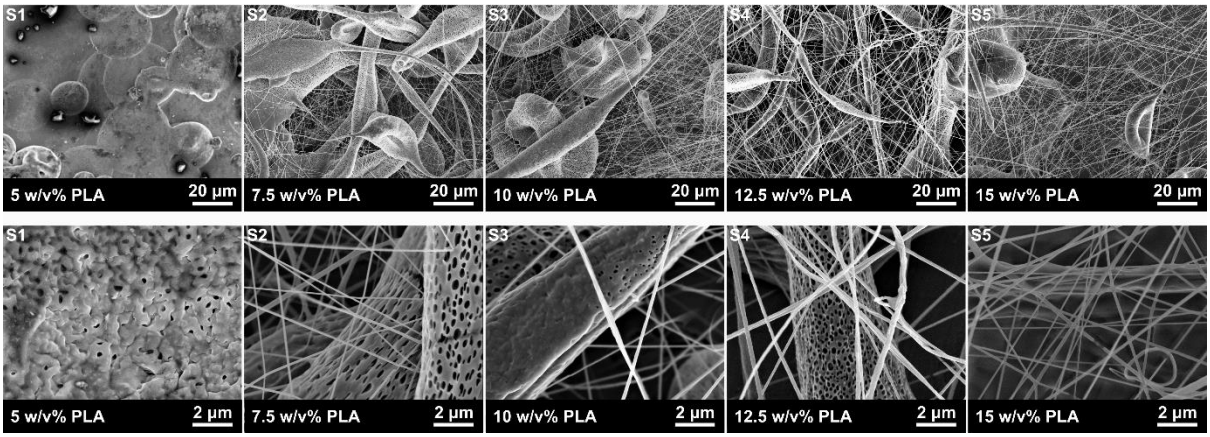

Figure S1. Scanning electron microscope (SEM) images of the electrosprayed/electrospun polylactic acid (PLA) microstructures/fibers at two different magnifications produced from various polymer concentrations, S1, S2, S3, S4, and S5, represent the electrospun PLA supports with 5, 7.5, 10, 12.5, and 15 w/v% PLA polymer concentration, respectively (Table 1 in the main text). The salt additive concentration was 0 w/w%, the applied voltage was 15 kV, the flow rate was 0.5 mL h^{-1}, and the tip-to-collector distance (TCD) was 100 mm.

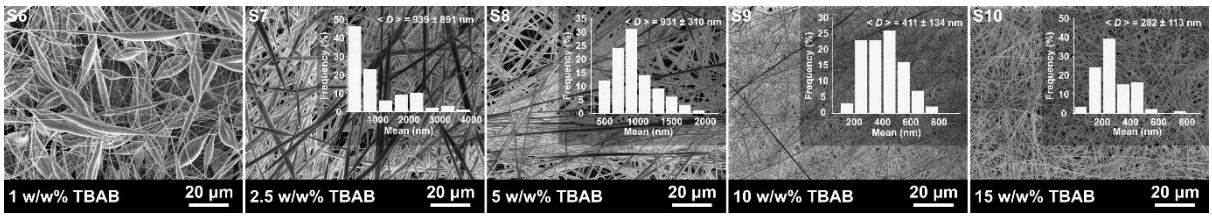

Figure S2. SEM images of the electrospun PLA fibers produced at different salt addition concentrations, S6, S7, S8, S9, and S10, represent the electrospun PLA supports with 1, 2.5, 5, 10, and 15 w/v% Tetrabutylammonium bromide (TBAB), respectively (Table 1 in the main text). The constant polymer concentration was 12.5 w/v% (with respect to the solvent), and the insets show the fiber size distributions. The applied voltage was 15 kV, the flow rate was 0.5 mL h^{-1}, and the TCD was 100 mm.

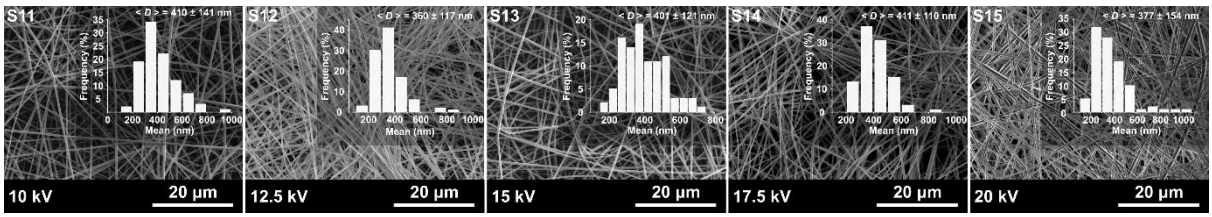

Figure S3. SEM images of the fabricated PLA fibers under different applied voltages, S11, S12, S13, S14, and S15, represent the PLA supports electrospun under 10, 12.5, 15, 17.5, and 20 kV, respectively (Table 1 in the main text), at a fixed polymer solution composition (12.5 w/v% PLA based on solvent and 10 w/w% TBAB based on PLA content). The insets show the fiber size distributions. The flow rate was 0.5 mL h^{-1}, and the TCD was 100 mm.

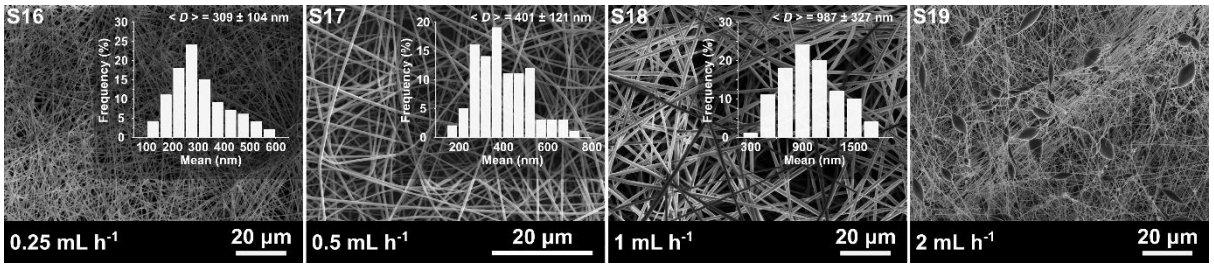

Figure S4. SEM images of the fabricated PLA fibers under different flow rates, S16, S17, S18, and S19, represent the PLA supports electrospun under the flow rates of 0.25, 0.5, 15, 1, and 2 mL h^{-1}, respectively (Table 1 in the main text), at a fixed polymer solution composition (12.5 w/v% PLA based on solvent and 10 w/w% TBAB based on PLA content) at 15 kV. The insets show the fiber size distributions. The TCD was 100 mm.

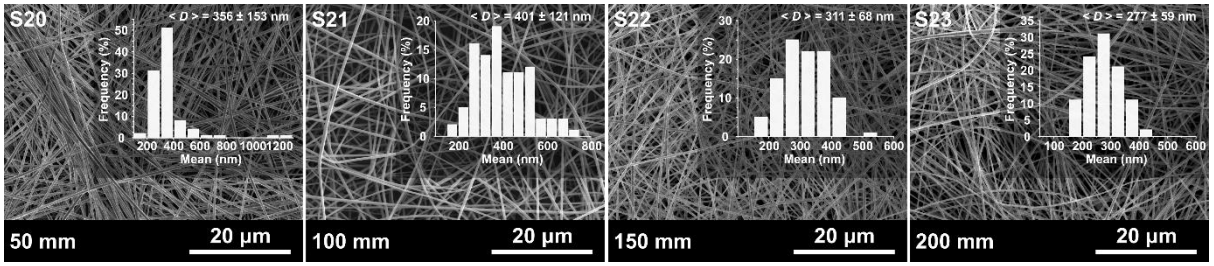

Figure S5. SEM images of the fabricated PLA fibers under different TCDs, S20, S21, S22, and S23, represent the PLA supports electrospun under TCDs of 50, 100, 150, and 200 mm, respectively (Table 1 in the main text), at a fixed polymer solution composition (12.5 w/v% PLA based on solvent and 10 w/w% TBAB based on PLA content) at an applied voltage of 15 kV and an injection flow rate of 0.5 mL h^{-1}. The insets show the fiber size distributions.

S2. Polymer solubility testing

Table S1. h–PLA support solubility in different organic solvents: √ means the support being stable in the solvent, o represents severe swelling, while × means dissolution.

Solvent	Density	Viscosity	Dielectric constant	UV	Refractive index	Hsp	Soluble
NMP	1.028	1.67	32	285	1.47	23	o
DMAc	0.937	2.14	37.8	268	1.438	22.8	o
DMF	0.944	0.92	36.6	268	1.43	24.9	o
DMSO	1.1	2.24	46.7	268	1.479	26.7	o
THF	0.889	0.55	7.6	212	1.407	19.5	×
MeTHF	0.854	0.558	6.97	-	1.406	18.1	√
MeOH	0.791	0.55	32.6	205	1.329	29.6	√
EtOH	0.816	1.1	25.55	205	1.363	26.5	√
IPA	0.786	2.86	18.3	21	1.377	23.6	√
MEK	0.805	0.42	18.5	329	1.379	19.05	√
Acetone	0.791	0.32	20.7	330	1.359	19.9	√
Acetonitrile	0.786	0.37	37.5	190	1.344	24.4	√
Ethyl acetate	0.902	0.46	6.02	256	1.372	18.2	√
Toluene	0.865	0.59	2.4			18.2	o

S3. Membrane swelling testing

Table S2. Swelling test results of the h–PLA support (each sample was measured thrice).

Solvents	dry weight m_1 (mg)			wet weight m_2 (mg)			Δm after 24 h			*R*s%		
	1	2	3	1	2	3	1	2	3	1	2	3
DMF	9.34	9.34	9.33	58.83	58.84	58.85	49.49	49.50	49.51	530.13	530.26	530.34
DMSO	8.47	8.49	8.47	47.43	47.44	47.45	38.96	38.95	38.98	459.62	459.55	459.88
MeCN	11.80	11.81	11.80	24.75	24.67	24.60	12.95	12.86	12.79	109.70	108.91	108.37
Acetone	13.09	19.10	13.09	57.83	57.67	57.48	44.73	38.57	44.39	296.41	255.56	294.14
MEK	8.05	8.06	8.05	17.77	17.75	17.76	9.71	9.70	9.71	120.60	120.40	120.50
EtOH	13.54	13.54	13.55	65.48	65.42	65.38	51.93	51.88	51.83	383.42	383.03	382.65
Toluene	10.64	10.63	10.63	68.92	68.82	68.73	58.28	58.19	58.10	548.23	547.41	546.51
Heptane	12.73	12.74	12.74	41.73	41.68	41.65	29.01	28.94	28.91	227.75	227.27	227.01

Table S3. Swelling test results of the free-standing selective layer (each sample was measured thrice).

Solvents	dry weight m_1 (mg)			wet weight m_2 (mg)			*Δ*m after 24 h			*R*s%		
	1	2	3	1	2	3	1	2	3	1	2	3
DMF	12.93	12.93	12.93	26.81	26.74	26.72	13.88	13.81	13.79	107.32	106.82	106.60
DMSO	7.54	7.54	7.54	17.33	17.42	17.74	9.80	9.89	10.20	129.99	131.20	135.40
MeCN	4.69	4.69	4.70	4.73	4.72	4.72	0.04	0.03	0.03	0.77	0.68	0.62
Acetone	6.12	6.11	6.12	6.35	6.32	6.30	0.23	0.21	0.18	3.78	3.42	3.01
MEK	4.92	4.92	4.91	5.37	5.37	5.61	0.46	0.45	0.69	9.29	9.24	14.13
EtOH	5.17	5.17	5.18	5.89	5.76	5.64	0.71	0.59	0.47	13.80	11.37	9.06
Toluene	5.88	5.88	5.88	7.66	7.39	7.24	1.78	1.51	1.37	30.27	25.70	23.26
Heptane	5.11	5.11	5.11	5.15	5.15	5.15	0.04	0.04	0.03	0.84	0.74	0.67

S4. Green nanofibrous support characterization

The dynamic mechanical analysis of the optimized PLA support and the h–PLA support was performed five times (from different places of the whole support), and the mean value and error were obtained.

Table S4. Mechanical properties of the optimized h–PLA support and the PLA support.

Sample name	Tensile strength (MPa)	Young's modulus (MPa)	Elongation at break (%)
h–PLA support	4.55 ± 0.82	60.12 ± 6.27	82.34 ± 11.11
PLA support	1.62 ± 0.23	25.36 ± 1.57	34.28 ± 2.94

S5. Biodegradation of the optimized h–PLA support

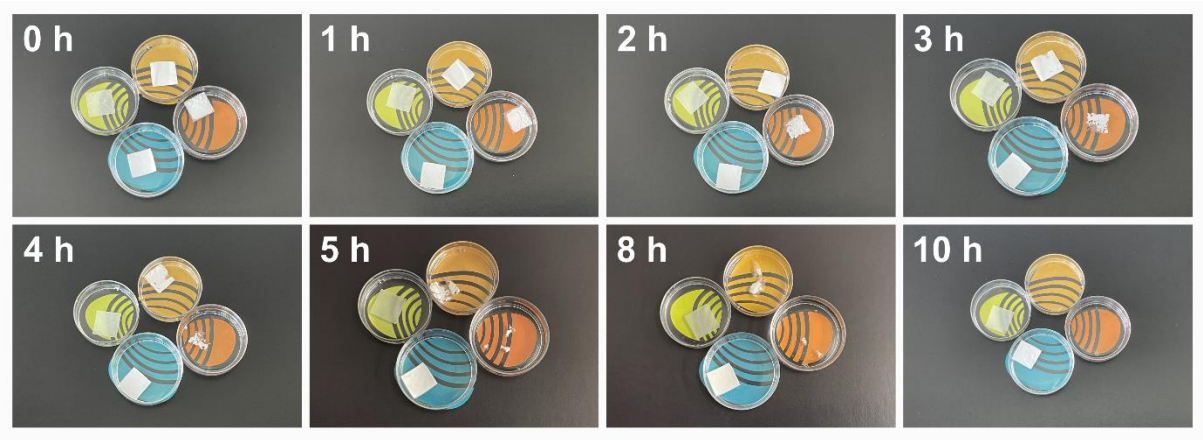

Figure S6. Biodegradability of the optimized h–PLA supports in 10 h: the orange dish (top) and the red dish (right) contain the h–PLA support with 200 μg mL^{-1} Proteinase K in 0.05 M Tris buffer solution, the blue dish (down) has the h–PLA support but with Type II water, while the green plate (left) contains the PP membrane with Proteinase K in 0.05 M Tris buffer solution.

S6. Optimization of gelatin concentration

Table S5. G–h–PLA supports with different gelatin concentrations (the solvent was water, and the support was h–PLA).

G–h–PLA	$C_{gelatin}$ (w/v%)
G0	0
G1	1
G2	2
G3	3
G4	4
G5	5

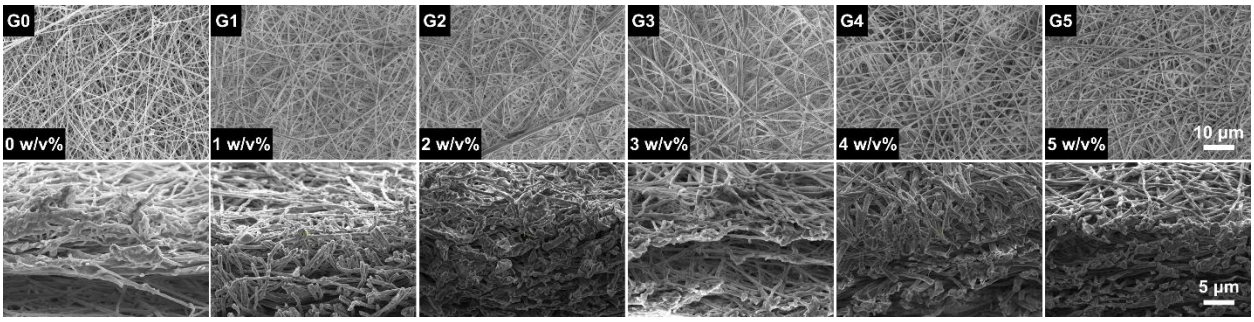

Figure S7. Surface and cross-sectional SEM images of the h–PLA support and the gelation interlayer supports with different gelatin concentrations.

S7. Reaction mechanism of Genipin–Priamine cross-linking

Due to the presence of the ester group on the genipin molecule, the S_N2 nucleophilic substitution of an amine group is observed during the cross-linking process [1]. Consequently, an intermediate aldehyde group is formed by an initial nucleophilic attack on genipin from a primary amine group. Subsequently, this aldehyde group is attacked by the secondary amine resulting from the previous step; therefore, the dihydropyran ring is opened [2]. Based on this, a heterocyclic compound of genipin linked to the priamine residue is formed.

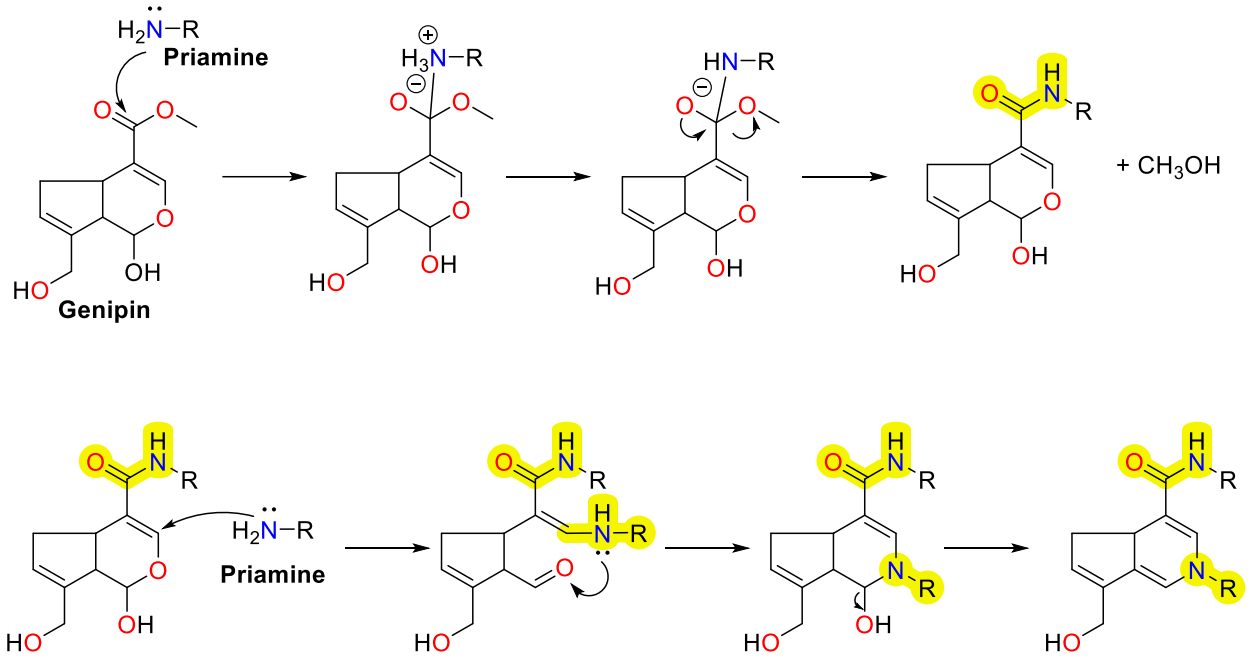

Figure S8. Two-step cross-linking mechanism of genipin and priamine.

S8. Chemical characterization of TFC membranes by XPS

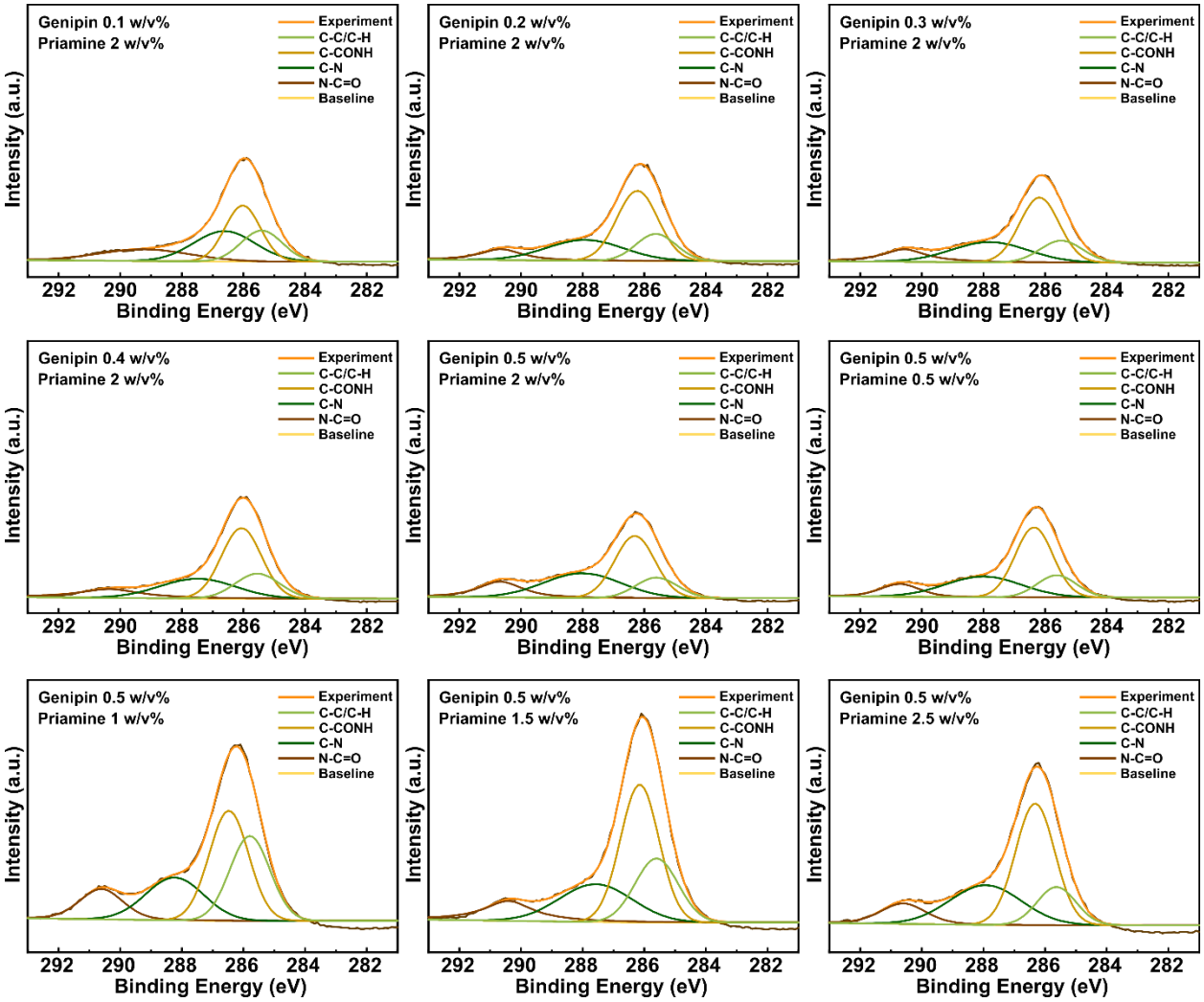

Figure S9. X-ray photoelectron spectroscopy (XPS) C 1s narrow scan results of green thin-film composite (TFC) membranes prepared with different genipin and priamine concentrations.

Table S6. Convoluted XPS narrow scanning C 1s peaks for each membrane (Table 2 in the main text).

	Peaks area				SUM	Ratio			
	N–C=O	C–N	C–CONH/C–COO	C–H/C–C		N–C=O	C–N	C–CONH/C–COO	C–H/C–C
M6	642.9296	1112.72	1184.327	764.246	3704.223	17.3567	30.0392	31.9723462	20.6317
M7	547.8901	1137.903	1496.74	511.0872	3693.62	14.8334	30.8073	40.522306	13.837
M8	481.7604	930.3508	1532.714	555.0428	3499.868	13.7651	26.5825	43.7934802	15.859
M9	475.7448	894.7207	1685.261	666.0182	3721.745	12.7828	24.0404	45.2814741	17.8953
M2	386.0634	958.137	1724.787	645.2721	3714.26	10.3941	25.7962	46.4368946	17.3728
M10	852.3339	1474.101	2591.139	2026.341	6943.915	12.2745	21.2287	37.3152465	29.1815
M11	869.0316	1648.61	3175.64	1648.083	7341.365	11.8375	22.4565	43.2568058	22.4493
M12	347.5492	941.7687	1581.274	520.9391	3391.531	10.2476	27.7682	46.6241942	15.36
M13	618.6356	1701.462	2858.182	890.5386	6068.818	10.1937	28.0361	47.0961891	14.674

S9. Priamine structure

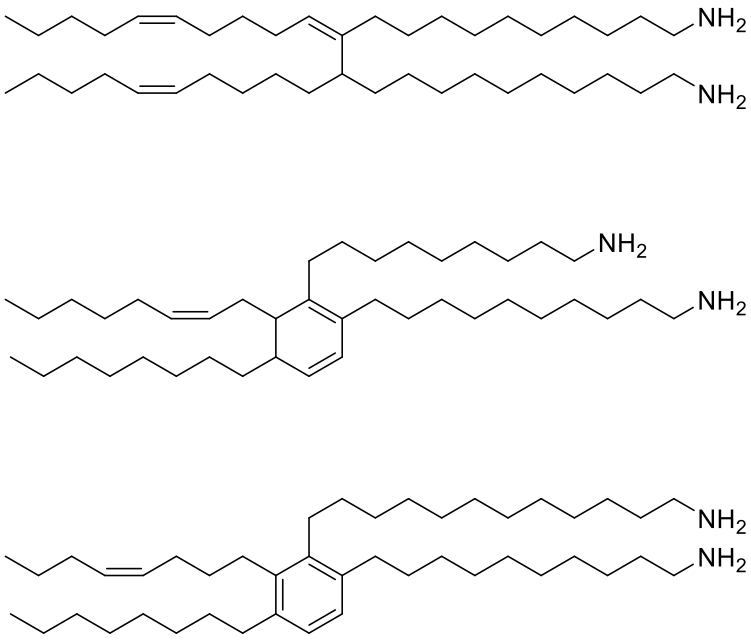

Figure S10. Commercial priamine with different structures.

S10. TFC membrane optimization

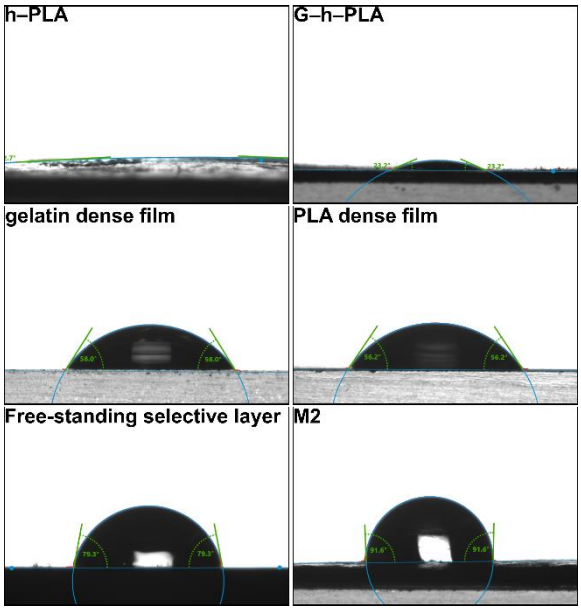

Figure S11. Water contact angle on the electrospun green support h–PLA, the support with interlayer G–h–PLA, the gelatin dense film, the PLA dense film, the free-standing selective layer, and M2. All the results were taken after 10 s when the water drop touched the surface.

Table S7. Free-standing (FS) selective layer fabrication with different monomer concentrations. The solvent for the genipin aqueous phase was water, and it was eucalyptol for the priamine organic phase.

Selective layer	$C_{Genipin}$ (w/v%)	$C_{Priamine}$ (w/v%)
FS1	0.1	2
FS2	0.2	2
FS3	0.3	2
FS4	0.4	2
FS5	0.5	2
FS6	0.5	0.5
FS7	0.5	1
FS8	0.5	1.5
FS9	0.5	2.5

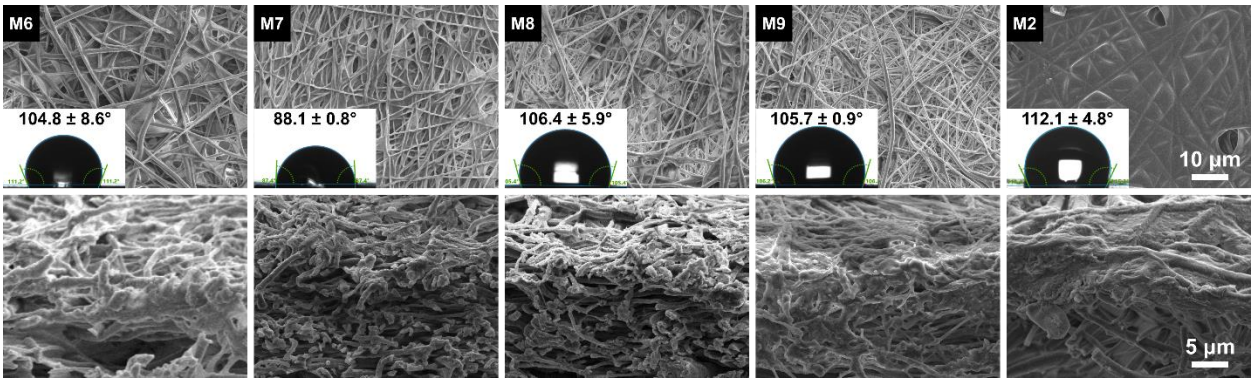

Figure S12. Surface and cross-sectional SEM images of green TFC membranes fabricated with different genipin concentrations. The insets show the water droplets on the respective TFC membranes.

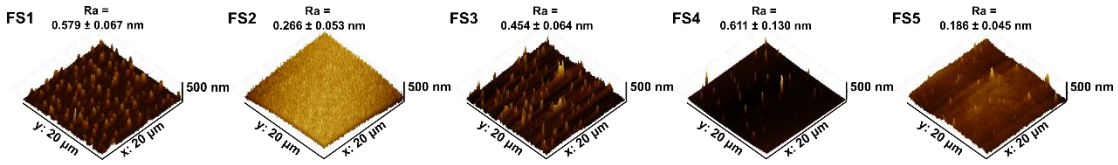

Figure S13. Atomic force microscope (AFM) images of free-standing thin films prepared with different genipin concentrations.

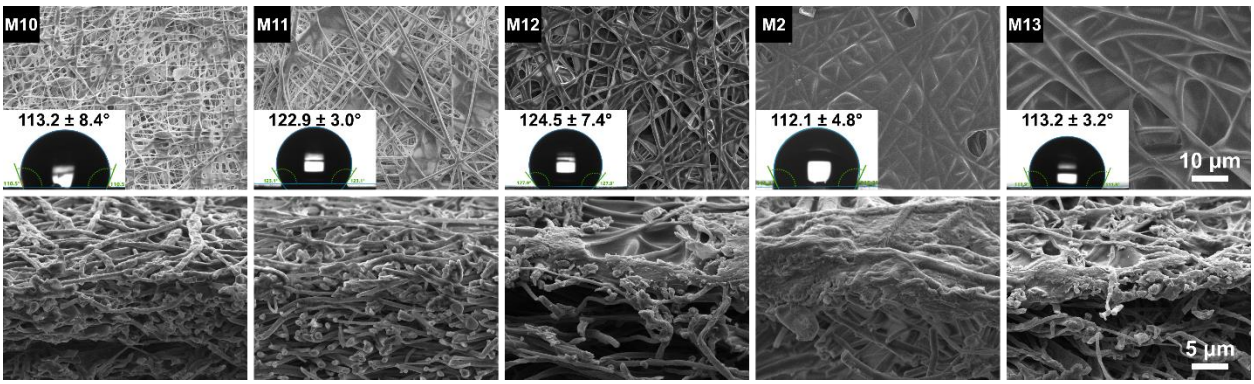

Figure S14. Surface and cross-sectional SEM images of green TFC membranes fabricated with different priamine concentrations.

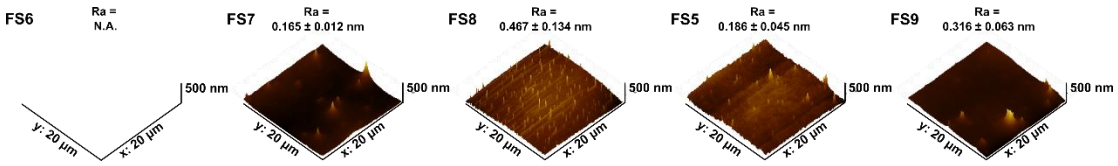

Figure S15. AFM images of free-standing thin films prepared with different priamine concentrations.

S11. Pore size calculation

Table S8. Physical properties of acetone [3].

Solvent	M_w[a] (Da)	d_m[b] (nm)	H[c] (mPa s)	V_m[d] (cm^3 mol^{-1})	ρ[e] (g ml^{-1})	δ$_d$[f] (MPa$^{0.5}$)	δ$_P$[g] (MPa$^{0.5}$)	δ$_h$[h] (MPa$^{0.5}$)	δ$_t$[i] (MPa$^{0.5}$)
AcMe	58.08	0.308	0.316	74.166	0.784	15.5	10.4	7.0	19.9

[a] Molar mass; [b] diameter; [c] dynamic viscosity; [d] molar volume; [e] density; [f,g,h,I] Hansen parameters (dispersion, polar, hydrogen bonding, and total, respectively).

As suggested by Livingston et al., the permeance of a solvent can be correlated with its physical properties [4]. The diameter of acetonitrile is calculated as follows.

$$d_{\mathrm{m}} = 2 \cdot \left(\frac{3V_m}{4\pi N_A}\right)^{\frac{1}{3}}, \quad \text{S1}$$

where V_{m} is the molar volume obtained from the solvent density and N_A is Avogadro's number. The Hagen–Poiseuille equation defines the volumetric flux (J_v) through a membrane comprising uniform capillaries as follows.

$$J_{v,i} = \frac{r_i^2 \Delta P \varepsilon}{8\mu_0 l}, \quad \text{S2}$$

where ε is the porosity, ΔP is the transmembrane pressure, l is the capillary length, μ_0 is the solvent bulk viscosity, and r_i is the capillary radius. Using the pore flow rate ($Q_{p,i}$), the flow through a pore with the radius r_i can be calculated as follows.

$$Q_{p,i} = \frac{\pi r_i^4 \Delta P}{8\mu_0 l}. \quad \text{S3}$$

The overall solute rejection can be calculated using the following equations.

$$R_{ij} = 1 - \frac{\Phi_{ij} K_{c,ij}}{1 - \left(1 - \Phi_{ij} K_{c,ij}\right)\left(\exp(-P_{e,ij})\right)}, \quad \text{S4}$$

where Φ_{ij} is the partition coefficient, $K_{c,ij}$ is the solute convective factor, $K_{d,ij}$ is the diffusive hindrance factor, and λ_{ij} is the ratio between solute radius $r_{s,j}$ (subindex for a solute is j) and pore radius r_i (the subindex for a pore size class in the discrete method is i).

$$\Phi_{ij} = \left(1 - \lambda_{ij}\right)^2, \quad \text{S5}$$

$$\lambda_{ij} = \frac{r_{s,j}}{r_i}. \quad \text{S6}$$

Assuming that a steric interaction occurs between the solute and the pore wall, $K_{c,ij}$ and $K_{d,ij}$ are expressed as follows.

$$K_{c,ij} = \left(2 - \Phi_{ij}\right)\left(1 + 0.054\lambda_{ij} - 0.988\lambda_{ij}^2 + 0.44\lambda_{ij}^3\right), \quad \text{S7}$$

$$K_{d,ij} = 1 - 2.3\lambda_{ij} + 1.154\lambda_{ij}^2 + 0.224\lambda_{ij}^3. \quad \text{S8}$$

The Peclet number ($P_{e,ij}$) characterizing the pore flow is defined as

$$P_{e,ij} = \frac{K_{c,ij}}{K_{d,ij} D_{s,j}} \left(\frac{r_i^2 \Delta P}{8 \mu_{p,i}} \right). \quad \text{S9}$$

The diffusivity $D_{s,ij}$ of a solute with the radius $r_{s,j}$ is calculated using the Stokes–Einstein equation.

$$D_{s,ij} = \frac{kT}{6\pi \mu_{p,i} r_{s,j}}, \quad \text{S10}$$

where k is the Boltzmann constant and T is the temperature. The Wilke–Chang formula can be used to solve the above equation and estimate solute diffusivity as follows.

$$D_{s,ij} = 7.4 \times 10^{-8} \frac{T\sqrt{\phi M_{solv}}}{\mu_{p,i} V_{m,j}^{0.6}}, \quad \text{S11}$$

where M_{solv} is the molecular weight (M_w) of the solvent molecule, ϕ is a dimensionless solvent parameter, and $V_{m,j}$ is the solute molar volume (in $cm^3\ g\ mol^{-1}$). If the rejection value $R(r)$ is a continuous function of the pore radius r, PDF $f_R(r)$ is introduced to describe the pore size distribution.

$$f(r) = \frac{1}{r\sqrt{2\pi b}} \exp\left[-\frac{\left(\log(r/r^*) + b/2\right)^2}{2b} \right], \quad \text{S12}$$

where

$$b = \log\left[1 + \left(\frac{\sigma}{r^*} \right)^2 \right]. \quad \text{S13}$$

To calculate *f(r)*, the mean pore radius (r^*) and its standard deviation (σ) must be estimated. For simplification, the distribution function is truncated to r_{max}.

$$\frac{f'_R(r)}{f_R(r)} = \frac{1}{\int_0^{r_{max}} f_R(r)dr}. \quad \text{S14}$$

The overall rejection value over the pore radius range of $0 < r < r_{max}$ can then be calculated as follows.

$$R_j = \frac{\int_0^{r_{max}} f'_R(r) r^4 R(r)/\mu(r) dr}{\int_0^{r_{max}} f'_R(r) r^4/\mu(r) dr}. \quad \text{S15}$$

By implementing the above models, the mean pore size and its standard deviation can be fitted by minimizing the error.

S12. Solvent properties

Table S9. Hansen solubility parameter and the physical properties of the organic solvent used in this study.

Solvent	Molar diameter (d_m, nm)	Viscosity (η, cP) at 25°C	Hansen solubility parameter ($MPa^{1/2}$) δ_P (Intermolecular force)	$\delta_{p,s}\ \eta_s^{-1}\ d_{m,s}^{-2}$
Toluene	0.7	0.55	1.4	4.843
Ethanol	0.57	1.22	8.8	21.327
Methyl ethyl ketone	0.66	0.4	9	50.393
Acetone	0.62	0.3	10.4	84.547
Acetonitrile	0.55	0.34	18	160.822

S13. Oil-in-water filtration

Table S10. Oil-in-water filtration at different priamine concentrations.

Membrane	Mean oil removal efficiency (%)	Standard derivation	Water permeance ($L\ m^{-2}\ h^{-1}\ bar^{-1}$)	Standard derivation
M10	18.86	4.09	87.55	3.15
M11	57.55	3.08	16.39	0.91
M12	66.11	2.47	12.02	0.58
M2	93.55	2.35	7.51	0.4
M13	99.6	0.36	5.59	0.35

S14. Acetone permeance and styrene dimer rejection of the reported membranes

Table S11. Summary of integrally skinned asymmetric (ISA), TFC, and MMM membrane performance.

Sample No	Membrane type	Acetone permeance (L m^{-2} h^{-1} bar^{-1})	Styrene dimer rejection (%)	Ref.
1	ISA	0.3	9	[5]
2	ISA	0.32	99	[5]
3	ISA	1.03	91	[5]
4	ISA	1.05	99	[5]
5	ISA	2	95	[5]
6	ISA	4	92	[5]
7	ISA	6	80	[5]
8	ISA	7	75	[5]
9	ISA	0.97	99	[6]
10	ISA	0.76	97	[6]
11	ISA	1	89	[7]
12	ISA	1.5	77	[8]
13	TFC	7	99	[9]
14	TFC	8.5	97	[9]
15	TFC	0.2	98	[9]
16	TFC	0.42	97.5	[9]
17	TFC	2.5	95	[5]
18	MMM	1.04	90	[5]
19	MMM	0.9	90	[10]
20	MMM	1.3	90	[5]
21	chitosan green TFC	31.7	60.455	[11]
22	chitosan green TFC	6.85	86.23	[11]

S15. Sustainability evaluation

Table S12. Total mole number of petroleum-based monomers.

No.	Monomer & additive	Mole number (mmol)	Total mole number (mmol)	Application	Reference
0	Genipin	1.1	2.7	OSN	This work
	Priamine	1.6			
1	Resorcinol	19	19.8	OSN	[9]
	Trimesoyl chloride	0.8			
2	m-Phenylenediamine	19	39.8	FO	[12]
	Trimesoyl chloride	0.4			
	Sodium dodecyl sulfate	0.4			
	Triethylamine	20			
3	m-Phenylenediamine	14	14.2	RO	[13]
	Trimesoyl chloride	0.2			
4	m-Phenylenediamine	37	40.8	RO	[14]
	Trimesoyl chloride	3.8			
5	m-Phenylenediamine	19	19.4	OSN	[15]
	Trimesoyl chloride	0.4			
6	Piperazine	6	9.5	NF	[16]
	3,3'5,5'-iphenyl tetraacyl chloride	0.3			
	Sodium hydroxide	3			
	Sodium dodecyl sulfate	0.2			
7	Piperazine	24	24.8	NF	[17]
	Trimesoyl chloride	0.8			
8	Piperazine	4	9	NF	[18]
	Trimesoyl chloride	0.8			
	N-aminoethyl Piperazine Propane Sulfonate	4.2			
9	m-Phenylenediamine	19	66.4	RO	[19]
	Trimesoyl chloride	0.4			
	Dimethyl sulfoxide	26			
	Triethylamine	11			
	Camphorsulfonic acid	10			
10	m-Phenylenediamine	19	45.1	NF	[20]
	Trimesoyl chloride	0.4			
	Triethylamine	24			
	Sodium dodecyl sulfate	1.7			
11	Polyethyleneimine	84.4	87	NF	[21]
	Trimesoyl chloride	2.6			
12	Polyethyleneimine	23.5	24	OSN	[22]

	Isophthaloyl dichloride	0.5			
13	Piperazine Trimesoyl chloride	2.3 0.8	3.1	NF	[23]
14	Piperazine Trimesoyl chloride	23.2 0.8	24	NF	[24]
15	m-Phenylenediamine Trimesoyl chloride	33.6 0.6	34.2	OSN	[25]
16	m-Phenylenediamine Trimesoyl chloride	18.9 0.4	19.3	OSN	[26]
17	m-Phenylenediamine Trimesoyl chloride	11.6 0.4	12	OSN	[27]
18	m-Phenylenediamine Trimesoyl chloride	18.5 0.4	18.9	OSN	[28]
19	m-Phenylenediamine Trimesoyl chloride	18.5 0.4	18.9	OSN	[29]
20	Polyethyleneimine Isophthaloyl dichloride Ethylenediamine	23.5 0.5 33.9	57.9	OSN	[30]
21	Resorcinol Trimesoyl chloride	19 0.8	19.8	OSN	[31]
22	m-Phenylenediamine Trimesoyl chloride Sodium dodecyl sulfate Triethylamine	19 0.4 0.4 20	39.8	OSN	[32]
23	m-Phenylenediamine Trimesoyl chloride	14 0.2	14.2	OSN	[33]
24	m-Phenylenediamine Trimesoyl chloride	37 3.8	40.8	OSN	[34]
25	m-Phenylenediamine Trimesoyl chloride	19 0.4	19.4	OSN	[35]

Table S13. Chemical hazards and toxicity of petroleum-based monomers used for TFC membrane fabrication.

No.	Monomer & Additive	Pictogram	Reference
0	Genipin Priamine		This work
1	Resorcinol Trimesoyl chloride		[9]
2	*m*-Phenylenediamine Trimesoyl chloride Sodium dodecyl sulfate Triethylamine		[12]
3	*m*-Phenylenediamine Trimesoyl chloride		[13]
4	*m*-Phenylenediamine Trimesoyl chloride		[14]
5	*m*-Phenylenediamine Trimesoyl chloride		[15]
6	Piperazine 3,3'5,5'-iphenyl tetraacyl chloride Sodium hydroxide Sodium dodecyl sulfate		[16]
7	Piperazine Trimesoyl chloride		[17]
8	Piperazine Trimesoyl chloride N-aminoethyl Piperazine Propane Sulfonate		[18]
9	*m*-Phenylenediamine Trimesoyl chloride Dimethyl sulfoxide Triethylamine Camphorsulfonic acid		[19]
10	*m*-Phenylenediamine Triethylamine Trimesoyl chloride Sodium dodecyl sulfate		[20]
11	Polyethyleneimine Trimesoyl chloride	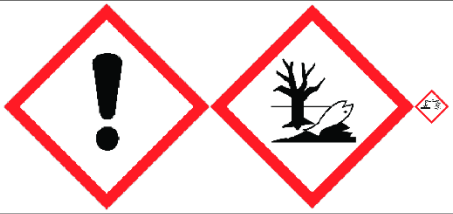	[21]

No.	Monomer & Additive	Pictogram	Reference
12	Polyethyleneimine Isophathalyol dicloride		[22]
13	Piperazine Trimesoyl chloride		[23]
14	Piperazine Trimesoyl chloride		[24]
15	*m*-Phenylenediamine Trimesoyl chloride		[25]
16	*m*-Phenylenediamine Trimesoyl chloride		[26]
17	*m*-Phenylenediamine Trimesoyl chloride		[27]
18	*m*-Phenylenediamine Trimesoyl chloride		[28]
19	*m*-Phenylenediamine Trimesoyl chloride		[29]
20	Polyethyleneimine Isophathalyol dicloride Ethylenediamine		[30]
21	Resorcinol Trimesoyl chloride		[31]
22	*m*-Phenylenediamine Trimesoyl chloride Sodium dodecyl sulfate Triethylamine		[32]
23	*m*-Phenylenediamine Trimesoyl chloride		[33]
24	*m*-Phenylenediamine Trimesoyl chloride		[34]
25	*m*-Phenylenediamine Trimesoyl chloride		[35]

= 1 mmol / 100 mL

Table S14. Total mole number of plant-based monomers.

No	Monomer & additive	Mole number (mmol)	Total mole number (mmol)	Application	Reference
0	Genipin	1.1	2.7	OSN	This work
	Priamine	1.6			
1	Tannic acid	0.06	2.25	NF	[36]
	Cyclohexane-1,4-diamine	2.19			
2	Tannic acid	0.06	0.55	OSN	[37]
	Terephthaloyl chloride	0.49			
3	Catechol	0.91	1.83	-	[38]
	m-Phenylenediamine	0.92			
4	Tannic acid	0.04	0.07	NF	[39]
	Trimesoyl chloride	0.03			
5	Quercetin	6.62	27.61	OSN	[40]
	Sodium hydroxide	20			
	Terephataloyl chloride	0.99			
6	Tannic acid	0.04	4.69	NF	[41]
	Polyethyleneimine	4.65			
7	Morin hydrate	6.75	7.74	OSN	[42]
	Terephataloyl chloride	0.99			
8	Catechin	6.89	27.09	OSN	[43]
	Sodium hydroxide	20			
	Terephataloyl chloride	0.2			
9	α-cyclodextrin	2.06	15.16	OSN	[44]
	Sodium hydroxide	12.35			
	Trimesoyl chloride	0.75			
10	Tannic acid	0.1	0.2	OSN	[45]
	Priamine	0.1			
11	Chitosan	0.5	3.5	OSN	[11]
	2,5-Furandicarboxaldehyde	3			

Table S15. Chemical hazards and toxicity of plant-based monomers for TFC membranes.

No.	Monomer & Additive	Pictogram	Reference
0	Genipin Priamine		This work
1	Tannic acid Cyclohexane-1,4diamine		[36]
2	Tannic acid Terephataloyl chloride		[37]
3	Catechol *m*-Phenylenediamine		[38]
4	Tannic acid Trimesoyl chloride		[39]
5	Quercetin Sodium hydroxide Terephataloyl chloride		[40]
6	Tannic acid Polyethyleneimine		[41]
7	Morin hydrate Terephataloyl chloride		[42]
8	Catechin Sodium hydroxide Terephataloyl chloride		[43]
9	α-cyclodextrin Sodium hydroxide Trimesoyl chloride		[44]
10	Tannic acid Priamine		[45]
11	Chitosan 2,5-Furandicarboxaldehyde		[11]

 = 1 mmol / 100 mL

Besides the presented sustainability analysis, the authors would like to mention the importance of techno-scientific context [46–48], which should be considered if the membranes are scaled up.

References

1. F.-L. Mi, H.-W. Sung and S.-S. Shyu, *J. Appl. Polym. Sci.*, 2001, **81**, 1700–1711.
2. M. F. Butler, Y.-F. Ng and P. D. A. Pudney, *J. Polym. Sci. A: Polym. Chem.*, 2003, **41**, 3941–3953.
3. J. R. Reimers and L. E. Hall, *J. Am. Chem. Soc.*, 1999, **121**, 3730–3744.
4. S. Karan, Z. Jiang and G. Livingston Andrew, *Science*, 2015, **348**, 1347–1351.
5. P. Marchetti, M. F. Jimenez Solomon, G. Szekely and A. G. Livingston, *Chem. Rev.*, 2014, **114**, 10735–10806.
6. X. X. Loh, M. Sairam, A. Bismarck, J. H. G. Steinke, A. G. Livingston and K. Li, *J. Membr. Sci.*, 2009, **326**, 635–642.
7. S. M. Dutczak, F. P. Cuperus, M. Wessling and D. F. Stamatialis, *Sep. Purif. Technol.*, 2013, **102**, 142–146.
8. X. X. Loh, M. Sairam, J. H. G. Steinke, A. G. Livingston, A. Bismarck and K. Li, *Chem. Commun.*, 2008, DOI: 10.1039/B815632H, 6324–6326.
9. M. F. Jimenez-Solomon, Q. Song, K. E. Jelfs, M. Munoz-Ibanez and A. G. Livingston, *Nat. Mater.*, 2016, **15**, 760–767.
10. H. Siddique, E. Rundquist, Y. Bhole, L. G. Peeva and A. G. Livingston, *J. Membr. Sci.*, 2014, **452**, 354–366.
11. S.-H. Park, C. Yang, N. Ayaril and G. Szekely, *ACS Sustain. Chem. Eng.*, 2022, **10**, 998–1007.
12. C. Klaysom, S. Hermans, A. Gahlaut, S. Van Craenenbroeck and I. F. J. Vankelecom, *J. Membr. Sci.*, 2013, **445**, 25–33.
13. W. Xie, G. M. Geise, B. D. Freeman, H.-S. Lee, G. Byun and J. E. McGrath, *J. Membr. Sci.*, 2012, **403-404**, 152–161.
14. S.-J. Park, S. J. Kwon, H.-E. Kwon, M. G. Shin, S.-H. Park, H. Park, Y.-I. Park, S.-E. Nam and J.-H. Lee, *Polymer*, 2018, **144**, 159–167.
15. M. F. Jimenez Solomon, Y. Bhole and A. G. Livingston, *J. Membr. Sci.*, 2012, **423–424**, 371–382.
16. H. Wang, Q. Zhang and S. Zhang, *J. Membr. Sci.*, 2011, **378**, 243–249.
17. M. Jahanshahi, A. Rahimpour and M. Peyravi, *Desalination*, 2010, **257**, 129–136.
18. Q.-F. An, W.-D. Sun, Q. Zhao, Y.-L. Ji and C.-J. Gao, *J. Membr. Sci.*, 2013, **431**, 171–179.
19. S. H. Kim, S.-Y. Kwak and T. Suzuki, *Environ. Sci. Technol.*, 2005, **39**, 1764–1770.
20. L. Shao, X. Q. Cheng, Y. Liu, S. Quan, J. Ma, S. Z. Zhao and K. Y. Wang, *J. Membr. Sci.*, 2013, **430**, 96–105.
21. D. Wu, Y. Huang, S. Yu, D. Lawless and X. Feng, *J. Membr. Sci.*, 2014, **472**, 141–153.
22. M. Peyravi, A. Rahimpour and M. Jahanshahi, *J. Membr. Sci.*, 2012, **423-424**, 225–237.
23. Y. Li, Y. Su, Y. Dong, X. Zhao, Z. Jiang, R. Zhang and J. Zhao, *Desalination*, 2014, **333**, 59–65.
24. N. Misdan, W. J. Lau, A. F. Ismail and T. Matsuura, *Desalination*, 2013, **329**, 9–18.
25. J. H. Kim, S. J. Moon, S. H. Park, M. Cook, A. G. Livingston and Y. M. Lee, *J. Membr. Sci.*, 2018, **550**, 322–331.
26. M. Namvar-Mahboub and M. Pakizeh, *Korean J. Chem. Eng.*, 2014, **31**, 327–337.
27. T.-D. Lu, B.-Z. Chen, J. Wang, T.-Z. Jia, X.-L. Cao, Y. Wang, W. Xing, C. H. Lau and S.-P. Sun, *Journal of Materials Chemistry A*, 2018, **6**, 15047–15056.
28. M. Namvar-Mahboub and M. Pakizeh, *Sep. Purif. Technol.*, 2013, **119**, 35-45.
29. M. F. Jimenez-Solomon, P. Gorgojo, M. Munoz-Ibanez and A. G. Livingston, *J. Membr. Sci.*, 2013, **448**, 102–113.

30. M. Peyravi, M. Jahanshahi, A. Rahimpour, A. Javadi and S. Hajavi, *Chem. Eng. J.*, 2014, **241**, 155–166.
31. S. Yang, Y. n. Xing, J. Zhang, B. Su, B. Mandal, X. Gao and C. Gao, *Desalin. Water Treat.*, 2019, **157**, 18–28.
32. S.-P. Sun, T.-S. Chung, K.-J. Lu and S.-Y. Chan, *AIChE J.*, 2014, **60**, 3623–3633.
33. S. H. Park, Y. J. Kim, S. J. Kwon, M. G. Shin, S. E. Nam, Y. H. Cho, Y. I. Park, J. F. Kim and J.-H. Lee, *ACS Appl. Mater. Interfaces*, 2018, **10**, 44050–44058.
34. P. H. H. Duong, D. H. Anjum, K.-V. Peinemann and S. P. Nunes, *J. Membr. Sci.*, 2018, **563**, 684–693.
35. L. Xia, J. Ren, M. Weyd and J. R. McCutcheon, *J. Membr. Sci.*, 2018, **563**, 857–863.
36. M. He, H. Sun, H. Sun, X. Yang, P. Li and Q. J. Niu, *Sep. Purif. Technol.*, 2019, **223**, 250–259.
37. L. Pérez-Manríquez, P. Neelakanda and K.-V. Peinemann, *J. Membr. Sci.*, 2017, **541**, 137–142.
38. W.-Z. Qiu, G.-P. Wu and Z.-K. Xu, *ACS Appl. Mater. Interfaces*, 2018, **10**, 5902–5908.
39. Y. Zhang, Y. Su, J. Peng, X. Zhao, J. Liu, J. Zhao and Z. Jiang, *J. Membr. Sci.*, 2013, **429**, 235–242.
40. M. H. Abdellah, L. Pérez-Manríquez, T. Puspasari, C. A. Scholes, S. E. Kentish and K.-V. Peinemann, *Adv. Sustain. Syst.*, 2018, **2**, 1800043.
41. Q. Li, Z. Liao, X. Fang, D. Wang, J. Xie, X. Sun, L. Wang and J. Li, *J. Membr. Sci.*, 2019, **584**, 324–332.
42. L. Pérez-Manríquez, P. Neelakanda and K.-V. Peinemann, *J. Membr. Sci.*, 2018, **554**, 1–5.
43. M. H. Abdellah, L. Pérez-Manríquez, T. Puspasari, C. A. Scholes, S. E. Kentish and K.-V. Peinemann, *J. Membr. Sci.*, 2018, **567**, 139–145.
44. J. Liu, D. Hua, Y. Zhang, S. Japip and T.-S. Chung, *Adv. Mater.*, 2018, **30**, 1705933.
45. S.-H. Park, A. Alammar, Z. Fulop, B. A. Pulido, S. P. Nunes and G. Szekely, *Green Chem.*, 2021, **23**, 1175–1184.
46. C. Ji, Z. Zhai, C. Jiang, P. Hu, S. Zhao, S. Xue, Z. Yang, T. He and Q. J. Niu, *Desalination*, 2021, **500**, 114869.
47. H. Wang, L. Wang, C. Liu, Y. Xu, Y. Zhuang, Y. Zhou, S. Gu, W. Xu and H. Yang, *Int. J. Biol. Macromol.*, 2019, **133**, 902–910.
48. N. More, M. Avhad and S. Utekar, *Polym. Bull.*, 2022 https://doi.org/10.1007/s00289-022-04135-z